High-Entropy Lattice Disordering Enhances Ion Migration in $LaCl_3$-Based Solid-State Electrolytes

Yongmei Zhou, Zhenyang Shen, Xiaozong Zhang, Can Ma, Qingtao Wang∗ and Yanxia Wu∗

a Key Laboratory of Eco-functional Polymer Materials of the Ministry of Education, Key Laboratory of Eco-environmental Polymer Materials of Gansu Province, College of Chemistry and Chemical Engineering, College of Engineering, Northwest Normal University, Lanzhou 730070, China

Qingtao Wang: wangqt@nwnu.edu.cn, Yanxia Wu: wuyx2014@nwnu.edu.cn

Materials and Synthesis

La^{3+} (1.032 Å, CN=9), In^{3+} (0.94 Å, CN=9), Zr^{4+} (0.84 Å, CN=9), Nb^{5+} (0.78 Å, CN=9) and Ta^{5+} (0.785 Å, CN=9) with their consistent coordination number (9) matching the $[LaCl_9]^{6-}$ polyhedron of the $LaCl_3$ matrix, and their ionic radii close to La^{3+} to ensure minimal lattice distortion and good lattice compatibility; meanwhile, the mixed valence states ($3^+/4^+/5^+$) of the doped ions can introduce appropriate La vacancies based on the charge neutrality principle, which not only constructs high-entropy disordered lattice but also forms 3D Li^+ transport channels, and these elements are selected for their moderate cost and excellent chemical stability in chloride systems, which are superior to other high-entropy cation combinations with large ionic radius differences or rare/expensive elements that would cause severe lattice distortion or increase synthesis cost. LiCl (99% AR, anhydrous, Macklin), $InCl_3$ (99%, anhydrous, Macklin), $ZrCl_4$ (98%, anhydrous, Macklin), $NbCl_5$ (≥ 99%, anhydrous, Macklin), and $TaCl_5$ (99%, anhydrous, Macklin) were used as the starting materials. The raw materials were weighed in stoichiometric proportions with a total mass of approximately 1 g. The mixed materials were thoroughly ground in an agate mortar for about 5 min. Subsequently, the mixed powder was sealed in a ZrO_2 jar with a ball-to-powder mass ratio (BPR) of 20:1, followed by high-speed ball milling at 1000 rpm for 15 h to obtain the product. Each milling cycle consisted of 30 min of operation and 10 min of resting to prevent overheating of the sample. The solid-state electrolyte (SSE) was further annealed: the SSE material was sealed in a quartz tube under vacuum, heated to 260 °C at a rate of 3 °C/min, and maintained at this temperature for 5 h. After annealing, the resulting SSE powder was transferred to a glovebox and manually ground into a fine powder for subsequent experimental applications. Both the grinding process and the subsequent sample transfer were performed in a glovebox (Ar atmosphere, H_2O < 0.01 ppm, O_2 < 0.01 ppm) to avoid moisture absorption or oxidation of the raw materials.

Structural Characterization

The crystal structure of the samples was characterized by an X-ray diffractometer (XRD, Bruker D8 ADVANCE, USA) with a Cu Kα radiation source (λ = 0.15416 nm). The scanning range for the conventional XRD test was set at 2θ=10°-60°. For data

collection dedicated to Rietveld refinement, the step size was 0.02° with a dwell time of 2 s per step, and the scanning range was extended to 2θ =10°-80°. To prevent the sample from reacting with moisture and oxygen in the air, the surface of the sample was covered with plastic wrap during the test. The XRD patterns were processed using the GSAS-II software combined with the Rietveld refinement method to obtain the crystal structure parameters of the samples. The surface morphology and element distribution of the material were analyzed via the combination of a field emission scanning electron microscope (FESEM, Thermo Fisher Apreo 2C, USA) and an energy dispersive X-ray spectrometer (EDS, Thermo Fisher Apreo 2C, USA). X-ray photoelectron spectroscopy (XPS, Thermo Fisher Scientific, Escalab 250Xi) was employed to investigate the chemical environment of various elements in the samples and observe the changes in the valence states of the elements before and after cycling.

Electrochemical Measurements

The impedance of the prepared samples was tested via electrochemical impedance spectroscopy (EIS) to calculate the ionic conductivity, using stainless steel blocking electrodes. The EIS measurements were performed on an electrochemical workstation (Autolab PGSTAT128N, Metrohm, Switzerland) with a frequency range of 1 MHz to 0.1 Hz and an applied perturbation voltage of 10 mV. Prior to testing, approximately 200 mg of the powder sample was loaded into a cylindrical mold with a diameter of 10 mm and pressed at 380 MPa to form a pellet-shaped solid electrolyte, with stainless steel rods used as electrodes on both sides. Subsequently, DC polarization tests were conducted. By applying external voltages of 0.1 V, 0.2 V, 0.3 V, 0.4 V, and 0.5 V respectively, the steady-state current within 60 minutes under constant voltage conditions was recorded to verify the ionic conduction mechanism. The final ionic conductivity (σ) was calculated using the following formula:

$$\sigma=d/(R\times S) \quad (1)$$

Where σ is the ionic conductivity, d is the thickness of the electrolyte pellet (measured using a micrometer), R is the impedance value of the electrolyte, and S is the contact area.

To further investigate the lithium-ion migration mechanism in the solid-state electrolyte, EIS measurements were performed at different temperatures to obtain the temperature-dependent ionic conductivity, thereby determining the activation energy (E_a) of the high-entropy SSE. The tests were conducted over a temperature range of 30 °C to 100 °C with an interval of 10 °C, and the obtained ionic conductivity data were fitted according to the classic Arrhenius equation:

$$\sigma=\frac{A}{T}\exp(-\frac{E_a}{K_bT}) \quad (2)$$

Where σ is the ionic conductivity, A is the pre-exponential factor, T is the thermodynamic temperature, E_a is the activation energy for ionic migration, and k_b is the Boltzmann constant with a value of 1.38×10^{-23} J K^{-1}.

Assembly and Testing of All-Solid-State Batteries

For the cathode of the all-solid-state battery (ASSB), single-crystal $Li(Ni_{0.83}Co_{0.07}Mn_{0.1})O_2$ (supplied by Guangdong Guande New Energy Technology Co., Ltd.) was adopted as the active material. It was thoroughly mixed and ground with solid electrolyte powder and a conductive additive (carbon black) at a mass ratio of 65:33:2 inside a glove box. Subsequently, the mixture was placed into a 2 mL polyethylene bottle, steel balls were added, and grinding was continued for 3 minutes using a grinder (JXMF-06, Shanghai Jinxin Instrument and Equipment Co., Ltd.) to prepare the composite cathode material. During battery assembly, 40 mg of Li_6PS_5Cl was first laid as the anode interface protection layer in a polyetheretherketone (PEEK) mold with a diameter of 10 mm and compacted under a pressure of 60.84 MPa. Then, 50 mg of the target electrolyte sample $Li(LaIn)_{0.25}(ZrNbTa)_{0.16}Cl_{4.74}$ was evenly spread on it and shaped by applying a pressure of 60.84 MPa again. After that, 5 mg of the composite cathode material was distributed on the surface of the solid electrolyte layer, followed by the third compaction. A lithium-indium alloy was used for the anode. The assembly sequence was as follows: an indium foil with a thickness of 0.02 mm and a diameter of 10 mm, and a lithium foil with a thickness of 0.03 mm and a diameter of 8 mm were sequentially placed on the surface of the Li_6PS_5Cl electrolyte. Finally, it was pressed and formed under a pressure of 91.26 MPa to obtain a structurally stable lithium-indium anode. The assembled all-solid-state batteries were subjected to electrochemical

performance tests at room temperature using the LAND CT2001A battery testing system (Wuhan LAND Electronics). The test voltage window ranged from 2.2 V to 4.5 V, and the test items included rate performance test and long-term cycle performance evaluation at a rate of 0.5 C.

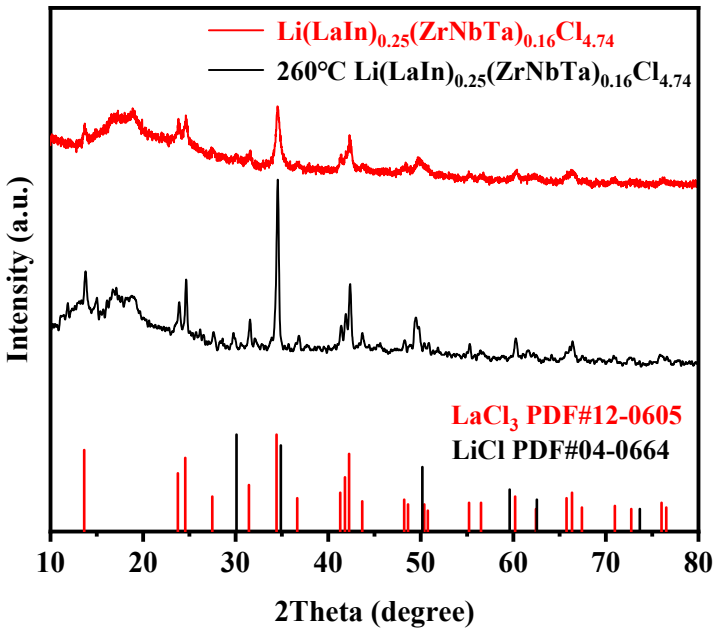

Fig S1. XRD Patterns of $Li(LaIn)_{0.25}(ZrNbTa)_{0.16}Cl_{4.74}$ after Ball Milling and Annealing at 260 °C.

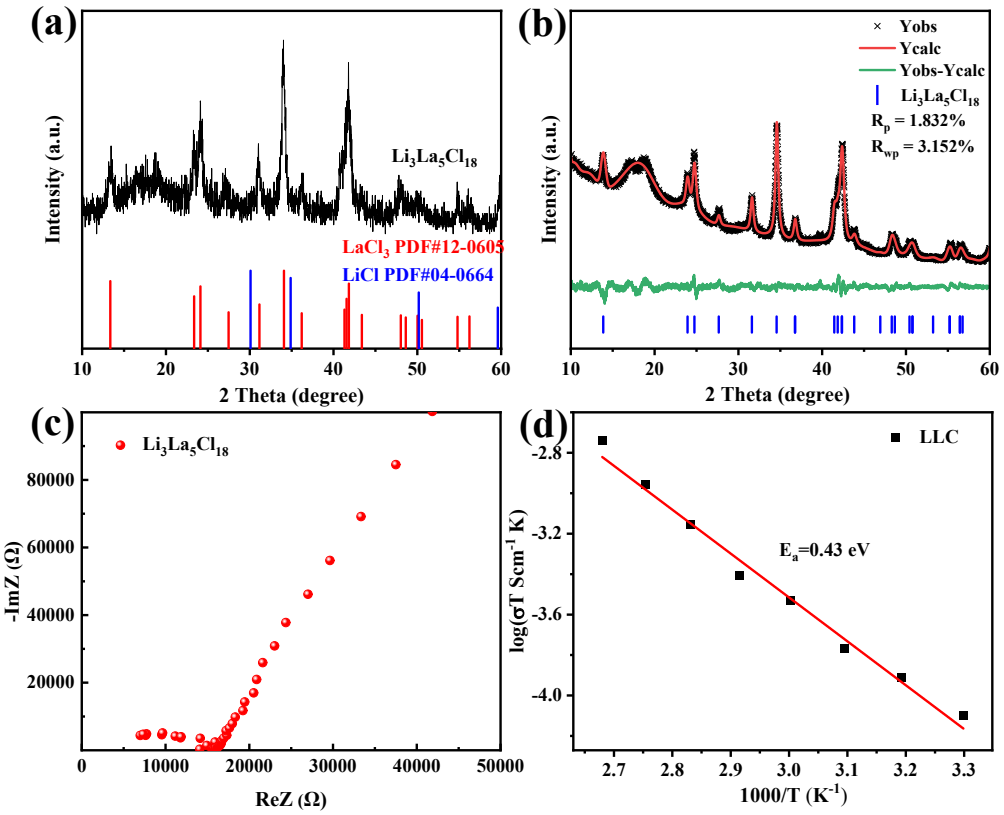

Fig S2. (a) XRD Pattern and Corresponding PDF Card of $Li_3La_5Cl_{18}$; (b) Rietveld Refinement Results of the XRD Pattern of $Li_3La_5Cl_{18}$; (c) Nyquist Plot of $Li_3La_5Cl_{18}$ at Room Temperature; (d) Activation Energy of $Li_3La_5Cl_{18}$ Fitted via Nyquist Plots at Different Temperatures

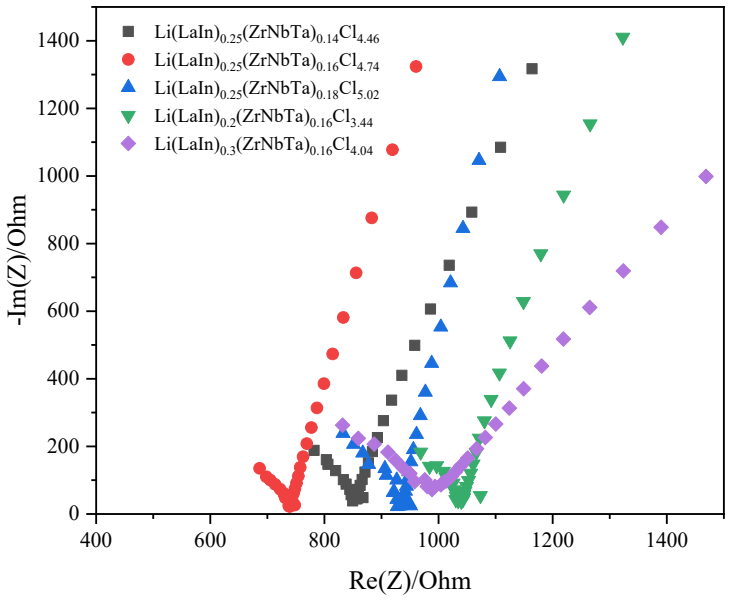

Fig S3. Nyquist Plots of $LaCl_3$-based High-Entropy SSEs with Different Ratios Before Annealing

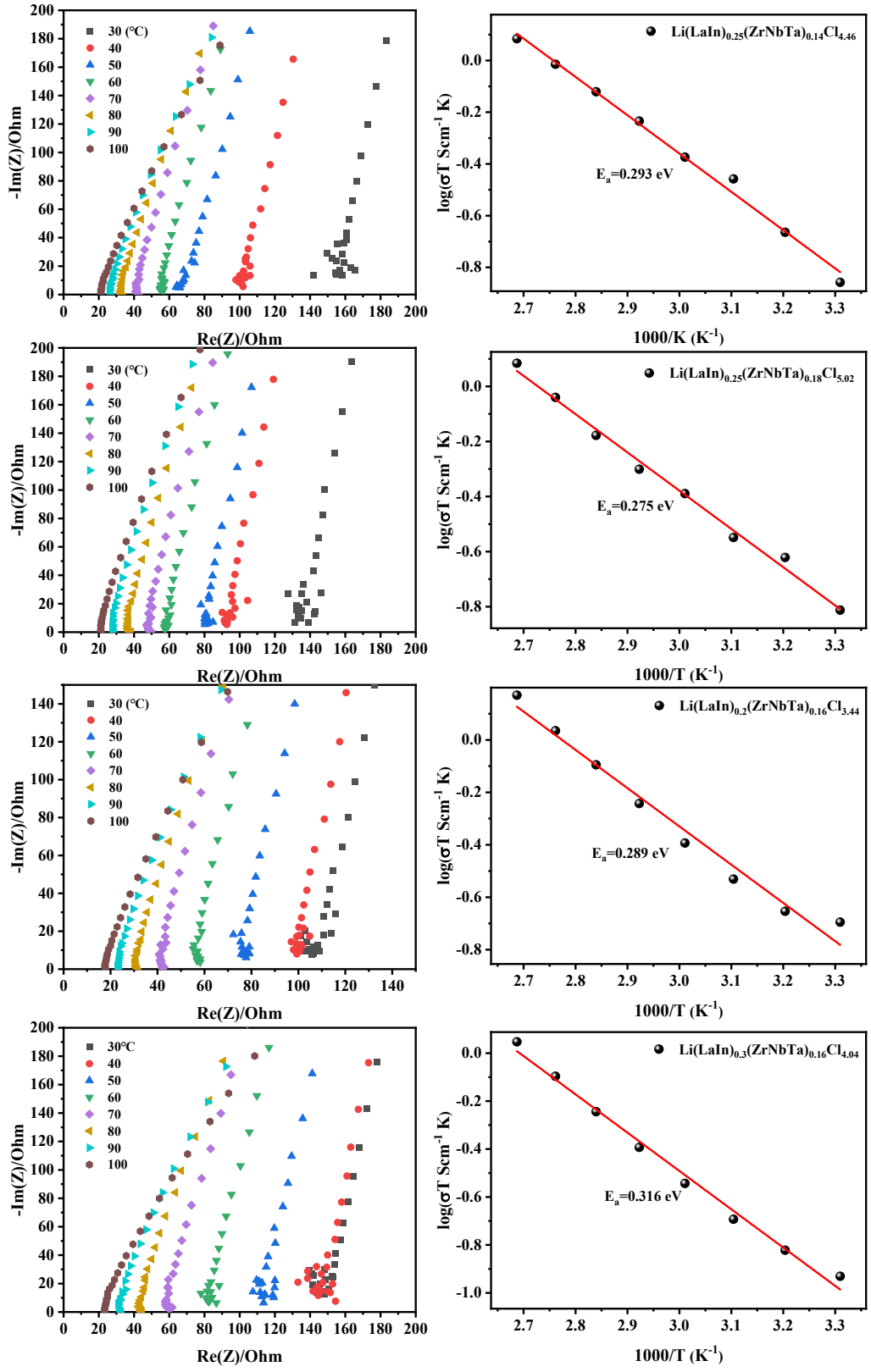

Fig S4. Nyquist Plots and Activation Energies of $Li(LaIn)_{0.25}(ZrNbTa)_{0.14}Cl_{4.46}$, $Li(LaIn)_{0.25}(ZrNbTa)_{0.18}Cl_{5.02}$, $Li(LaIn)_{0.2}(ZrNbTa)_{0.16}Cl_{3.44}$, and $Li(LaIn)_{0.3}(ZrNbTa)_{0.16}Cl_{4.04}$ at Different Temperatures

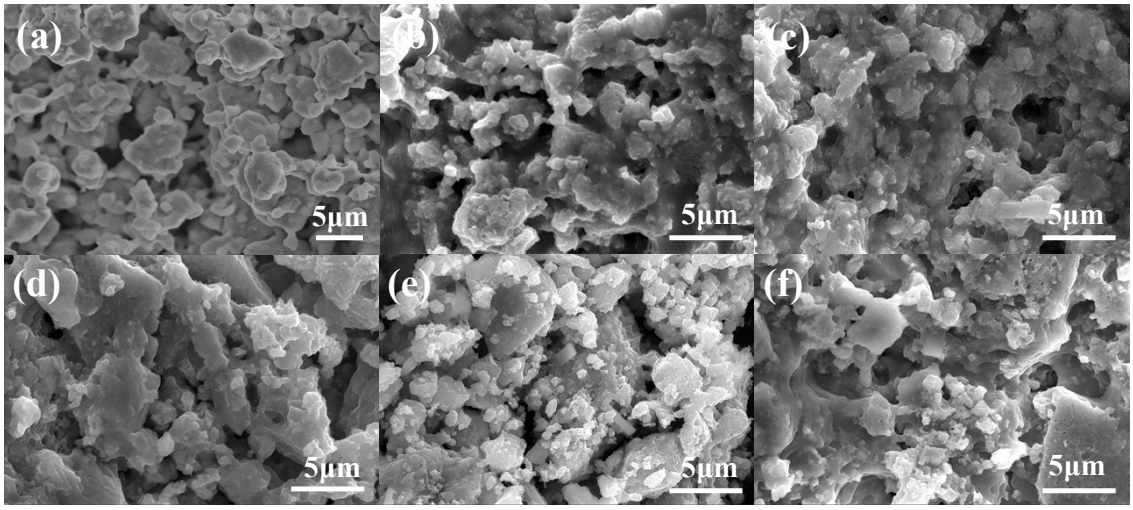

Fig S5. SEM Images of: (a) $Li_3La_5Cl_{18}$; (b) $Li(LaIn)_{0.25}(ZrNbTa)_{0.14}Cl_{4.46}$; (c) $Li(LaIn)_{0.25}(ZrNbTa)_{0.16}Cl_{4.74}$; (d) $Li(LaIn)_{0.25}(ZrNbTa)_{0.18}Cl_{5.02}$; (e) $Li(LaIn)_{0.2}(ZrNbTa)_{0.16}Cl_{3.44}$; (f) $Li(LaIn)_{0.3}(ZrNbTa)_{0.16}Cl_{4.04}$.

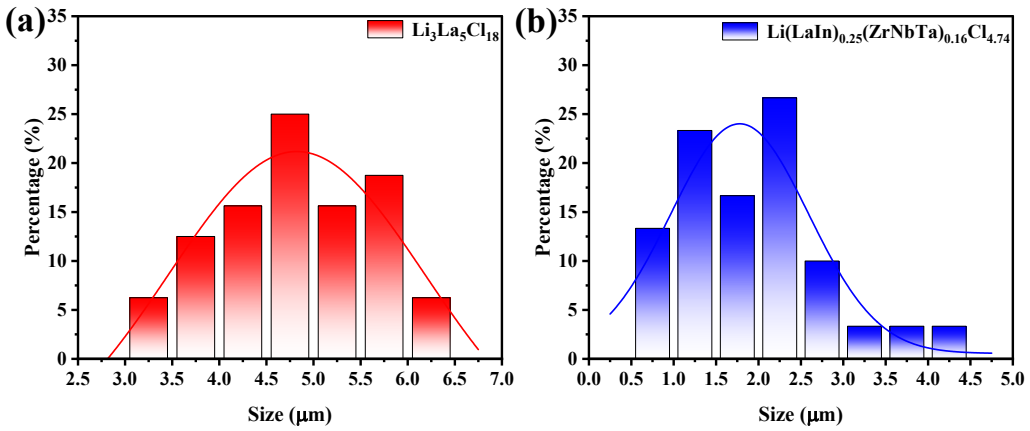

Fig S4. Histogram of the size distribution of $Li_3La_5Cl_{18}$ (a) and $Li(LaIn)_{0.25}(ZrNbTa)_{0.16}Cl_{4.74}$ (b).

Table S1. Rietveld Refinement Structural Data of $Li(LaIn)_{0.25}(ZrNbTa)_{0.16}Cl_{4.74}$ at Room Temperature

			x	y	z	Occ.	U	Site
1	Li	Li1	0.00000	0.00000	0.00000	0.236	0.010	2b
2	La	La1	0.33333	0.66667	0.25000	0.125	0.009	2c
3	In	In1	0.33333	0.66667	0.25000	0.125	0.009	2c
4	Zr	Zr1	0.33333	0.66667	0.25000	0.080	0.009	2c
5	Nb	Nb1	0.33333	0.66667	0.25000	0.080	0.009	2c
6	Ta	Ta1	0.33333	0.66667	0.25000	0.080	0.009	2c
7	Li	Li2	0.15774	0.66987	0.25000	0.088	0.010	6h
8	Cl	Cl1	0.37539	0.30529	0.25000	0.790	0.113	6h

Table S2. A comparison of the relevant literature on different high-entropy halide electrolytes.

Materials	Ionic conductivity (mS cm^{-1})	Activation energies (eV)	Test temperature (℃)	Ref.
HELa0.5 halide SSE	0.82	0.34	25	[1]
$Li_{2.6}$(Y，Ho，Er，Tm，Yb)$Cl_{5.6}$	0.52	0.41	25	[2]
$Li_{1.245}Al_{0.745}(ZrPSiB)_{0.0636}O_{0.7}Cl_{3.1}$	0.2	0.32	25	[3]
$Li(LaIn)_{0.25}(ZrNbTa)_{0.16}Cl_{4.74}$	0.51	0.265	25	this work

1. X. Hao, K. Chen, M. Jiang, Y. Tang, Y. Liu and K. Cai, *Chemical Engineering Journal*, 2025, **504**, 158963.

2. L. Luo, A. Zheng, Y. Yu, L. Li, S. Ma, S. Jin and J. Yu, *Nano Letters*, 2025, **25**, 13294-13300.

3. W. Xue, Y. Cui, Z. Long, H. Shan, N. Hu and S. Song, *Applied Physics Letters*, 2025, **127**.

Table S3. EDS quantitative analysis table of $Li(LaIn)_{0.25}(ZrNbTa)_{0.16}Cl_{4.74}$

Element	Line Type	Net Counts	Weight %	Atom %
Cl	K	820563	49.7	76.9
Zr	L	134346	11.7	7.0
Nb	L	30283	2.4	1.4
In	L	102156	13.6	6.5
La	L	116021	13.8	5.5
Ta	L	21224	8.8	2.7
			100.00	100.00